Michigan State University

National Superconducting Cyclotron Laboratory

FRAGMENT DISTRIBUTIONS FOR HIGHLY CHARGED SYSTEMS

C. WILLIAMS, W. G. LYNCH, C. SCHWARZ, M. B. TSANG, M. HUANG, W. C. HSI, D.R. BOWMAN, C. K. GELBKE, M. A. LISA, G. F. PEASLEE, L. PHAIR, D.O. HANDZY, J. DINIUS, M-C. LEMAIRE, S.R. SOUZA, G. VAN BUREN, R.J. CHARITY, L.G. SOBOTKA, G. J KUNDE, U. LYNEN, J. POCHODZALLA, H. SANN, W. TRAUTMANN, D. FOX, R.T. DE SOUZA, G. PEILERT, A. BOTVINA, N. CARLIN

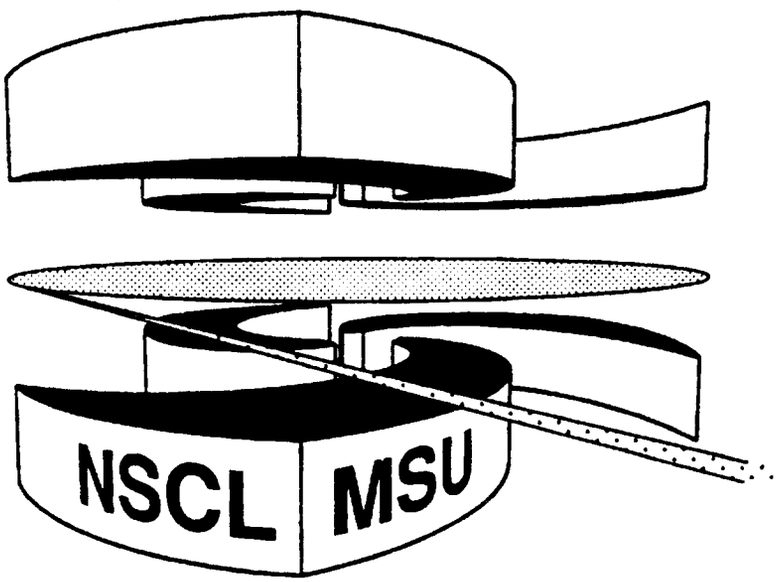

MSUCL-1019

MARCH 1996

Fragment Distributions for Highly Charged Systems

C. Williams, W.G. Lynch, C. Schwarz[a], M.B. Tsang, M.J. Huang, W.C. Hsi, D.R. Bowman[b], C.K. Gelbke, M.A. Lisa[c], G.F. Peaslee[d], L. Phair[c], D.O. Handzy[e], J. Dinius, *National Superconducting Cyclotron Laboratory and Department of Physics and Astronomy, Michigan State University, East Lansing, MI 48824,*

M-C. Lemaire, S. R. Souza, *Laboratoire National SATURNE, CEN Saclay, 91191 Gif-sur-Yvette, France,*

G. Van Buren, R.J. Charity, and L.G. Sobotka, *Department of Chemistry, Washington University, St. Louis, MO 63130,*

G.J. Kunde[f], U. Lynen, J. Pochodzalla[g], H. Sann, W. Trautmann, *Gesellschaft für Schwerionenforschung, Planckstr. 1, D-64291 Darmstadt, Germany,*

D. Fox[b], R.T. de Souza, *Department of Chemistry and IUCF, Indiana University, Bloomington, IN 47405,*

G. Peilert[h], *Lawrence Livermore National Laboratory, Livermore, CA 94550,*

A. Botvina[i], *Institute for Nuclear Research, Moscow, Russia,*

and

N. Carlin, *Instituto de Fisica, Universidade de São Paulo, CEP 01498, São Paulo, Brazil.*

Abstract

Charge and transverse energy distributions for intermediate mass fragments have been extracted for central $^{84}Kr+^{197}Au$ collisions at E/A= 35 - 400 MeV. The slopes of the measured fragment charge distributions decrease monotonically with incident energy, consistent with the expectations for highly charged systems but not with recent critical exponent analyses. Dynamical calculations do not accurately reproduce the fragment charge or transverse energy distributions. Statistical model calculations, which reproduce the experimental trends, suggest that post breakup fragment secondary decays alter significantly the observed charge distributions.

---

[a] Present Address: Gesellschaft für Schwerionenforschung, D-6100 Darmstadt 11, Germany.
[b] Present Address: Chalk River National Laboratories, Chalk River, Ontario, K0J1J0 Canada.
[c] Present Address: Lawrence Berkeley Laboratory, Berkeley CA.
[d] Present Address: Physics Department, Hope College, Holland MI.
[e] Present Address: Deloitte and Touche, New York NY.
[f] Present Address: NSCL Michigan State University, East Lansing, MI 48824, USA.
[g] Present Address: Max-Planck Institut für Kernphysik, Heidelberg Germany.
[h] Present Address: MB Informatik, Bayer AG, Leverküson, Germany.
[i] Present Address: Hahn-Meitner Institute, Berlin, Germany.

For infinite systems near a critical point, relationships between thermodynamic parameters are largely governed by a set of critical exponents [1,2]. Theoretical [3] and experimental prescriptions [4] for extracting critical exponents for the nuclear liquid-gas phase transition from nuclear collisions assume that the observed fragment mass distributions differ little from those for infinite nuclear matter near critical density, and therefore decrease most gradually with mass for reaction trajectories that pass through the critical point. The presence of long range Coulomb interactions, however, complicates the extrapolation of increasingly heavy laboratory systems towards the thermodynamic limit characteristic of critical phenomena [1,2]. Furthermore, post-breakup secondary decays [5] alter the observed fragment charge distributions. Both have been assumed to be negligible in previous analyses [4,6,7].

Assumptions underlying present critical exponent analyses of highly charged systems have been undermined by recent calculations [8-10]. Classical molecular dynamics calculations of highly charged systems predict a monotonic evolution of the fragment charge distributions, from flat distributions characterized by $Y(A) \propto A^{-\tau}$ with $\tau \approx 1$ at low excitation energies to steeply falling charge distributions at high excitation energies [8,10]. In contrast to corresponding calculations for neutral systems [9,11] and the assumptions of critical exponent analyses, a minimum in the value of τ, that could indicate critical phenomena, is not predicted for highly charged systems at moderate temperature [8,10]. Fragment yields may also be enhanced by a Coulomb driven evolution towards a bubble-like breakup geometry [12,13]. Consistent with these expectations, extremely flat charge distributions have been observed in central Au+Au collisions at E/A = 35 MeV [14], but predictions [8,10] for highly charged systems of a monotonic decrease of the slopes of the fragment charge distributions with incident energy have not been tested until now. Detailed comparisons of dynamical and statistical model calculations are also provided in this paper which reveal the charge distributions after secondary decay to be significantly steeper than those before secondary decay, rendering questionable present techniques [3,4,6,7] for critical exponent extraction.

The experimental data were measured using two different accelerators. Measurements at E/A = 35, 55, and 70 MeV were performed at the National Superconducting Cyclotron Laboratory of Michigan State University by bombarding gold targets of 1.3 mg/cm^2 by ^{84}Kr beams of 35A and 55A MeV and gold targets of 4 mg/cm^2 by ^{84}Kr beams of 70A MeV. Measurements at 100A, 200A, and 400A MeV were performed at the Laboratoire National SATURNE at Saclay by bombarding ^{84}Kr

beams on gold targets of 5 mg/cm^2 areal density. Charged particles were detected with the Miniball/Wall 4π array [15] consisting of 268 phoswich detectors covering $5.4° < \theta_{lab} < 160°$ with a geometric efficiency of approximately 90% of 4π.

Detectors with particle identification thresholds of $E_{th}/A \sim 4$ MeV (6 MeV) for Z=3 (Z=10) particles were constructed from 80 μm thick plastic scintillator foils and 3 cm thick CsI(Tl) crystals and used at forward angles, $5.4° \leq \theta_{lab} \leq 25°$. Detectors with particle identification (PID) thresholds of $E_{th}/A \sim 2$ MeV (4 MeV) for Z=3 (Z=10) particles were constructed from 40 μm thick plastic scintillator foils and 2 cm thick CsI(Tl) crystals and used at backward angles, $25° \leq \theta_{lab} \leq 160°$. Unit charge resolution up to $Z \approx 12$ was achieved for particles that traversed the fast plastic scintillator. Lithium ions that punched through the CsI(Tl) crystals were not counted as IMF's because they were not distinguished from light particles. To ensure accurate energy determination, low energy thresholds of E/A= 5 MeV were imposed in software on fragments of Z=3-8 respectively for the determination of $\langle E_t \rangle$ values. For consistency with ref. [16], charge distributions and fragment multiplicities were obtained using the software thresholds of ref. [16]. This information was used to project all the theoretical calculations, described herein, upon the experimental acceptance. A "reduced" impact parameter scale $\hat{b} = b/b_{max}$ was constructed from the charged particle multiplicity following refs. [16,17]; the constraint $\hat{b} \leq 0.25$ was applied to select central collisions. A value of $b_{max} = 10$ fm, determined by direct beam counting at E/A=200 MeV, provides an approximate impact parameter calibration.

The solid points in Fig. 1 show the fragment charge distributions for the six incident energies. These distributions decrease monotonically with fragment charge and can be approximately described by a power law of the form $Y(Z) = C \cdot Z^{-\tau}$. Using this functional form, fits for $3 \leq Z \leq 12$, shown by the solid lines, follow the experimental yields in the figure closely. The extracted values for τ are shown as the solid circles in the lower panel of Fig. 2. Consistent with the classical molecular dynamics calculations for highly charged systems [8,10] and contrary to the assumptions of critical exponent analyses, τ increases monotonically with incident energy and does not have a minimum at intermediate energies. The lowest value for τ ($\tau \approx 1.4$), attained at E/A=35 MeV, is somewhat more than half of the value $\tau \approx 2.3$ that is expected to characterize the mass distribution of a system at the critical point in the liquid-gas phase diagram [1,2].

Even though classical molecular dynamics simulations predict this trend, nuclei are quantal systems, and the question whether molecular dynamics models can reproduce such trends when the Pauli exclusion principal is taken into account remains relevant. To illustrate some of the difficulties with present semi-classical molecular dynamics calculations, we performed analogous fits of the charge distributions predicted by the Quantum Molecular Dynamics model of ref. [17] in which the Pauli principle is modeled by a repulsive "Pauli potential" acting in phase space. Fits to these calculations for $3 \leq Z \leq 12$, depicted by the dashed lines in the lower panel of Fig. 2, predict a much more gradual dependence of τ upon incident energy than is experimentally observed; even though the predicted fragment multiplicities (upper panel) [16] significantly underestimate the experimental values at E/A < 100 MeV. The crosses at E/A=50 MeV in the upper and lower panels of Fig. 2 correspond to calculations without the Pauli potential, using the same techniques as ref. [19]. In contrast to the findings of ref. [20], little sensitivity to the Pauli potential is observed in these simulations, indicating that the origin of the discrepancy between these theoretical and experimental charge distributions lies elsewhere.

Part of the discrepancy between theoretical and experimental fragment multiplicities and charge distributions at low incident energies may be traced to the prediction of hot residues within the QMD calculations which, due to the high heat capacities of classical systems [21], do not decay via fragment emission. Some of these discrepancies may be alleviated by allowing these residues to decay via statistical models [22,23]. The dot-dashed lines in Fig. 2 depict results obtained when fragments with $A \geq 4$ predicted by the QMD model with the Pauli potential at an elapsed time of t=200 fm/c are allowed to decay according to the statistical multifragmentation model (SMM) [16,24], which contains a "cracking" phase transition at low density. The larger values for τ which characterize the QMD+SMM calculations indicate that the corresponding fragment charge distributions are much steeper than those experimentally observed, even for incident energies E/A ≤ 100 MeV where the fragment multiplicities are well reproduced [16].

It is interesting to investigate whether the discrepancies between the measurements and the QMD+SMM calculations reflect a fundamental limitation of the SMM model or whether a satisfactory agreement might be obtained with reasonable though alternative input parameters. To explore this issue, SMM calculations were performed, varying the excitation energy, density, and collective flow of the fragmenting system. Since two-fragment correlations provide evidence that the

limit of a single freezeout time is not attained [25], only a fraction f_A of the total system having a fraction f_E of the total available excitation energy per nucleon is assumed to be equilibrated. The remaining excitation energy and mass of the system is assumed to be contained in a preequilibrium source that is too hot to emit fragments.

Collective motion influences the energy spectra and consequently the detection efficiency for fragments in the experimental array but is not apriori predicted by the SMM model. Previous investigations indicate that the attractive nuclear mean field can support a form of "rotational" flow at low incident energies [26]. At higher incident energies this rotational flow decreases and flow is primarily in an outward or "radial" direction [27] due to pressure from nucleon-nucleon collisions and from the high density nuclear equation of state in the central overlap region. To bracket these two limits, the influence of collective flow was estimated in the limits of purely collective rotational flow and purely collective radial expansion assuming a breakup density of ρ/ρ_o=1/6 [24,28].

Collective flow was explored by computing the mean transverse energy $\langle E_t \rangle = \Sigma_i E_i \sin^2\theta_i$, where E_i and θ_i are the kinetic energy and scattering angle of the i-th fragment. Experimental values for $\langle E_t \rangle$, shown as the solid points in Fig. 3, generally increase with incident energy and, except for the two highest energies, with the fragment mass. At E/A 400 MeV, however, a clear decrease of $\langle E_t \rangle$ with fragment mass is observed supporting the observations of refs. [27] that heavier fragments do not participate fully in the transverse expansion, due to a suppression of fragment formation in rapidly expanding nuclear systems [29]. SMM model calculations were performed with excitation energies per nucleon, equilibrium source sizes, and collective flow velocities that optimize the agreement with the fragment charge distributions, total fragment multiplicities, and transverse energies respectively. Calculations with two sets of optimized parameters, listed in Table 1and represented by the solid lines in Figs. 2 and 3, reproduce the experimental trends reasonably well. Virtually identical mean transverse energies are obtained via calculations with parameter set 1 which assumes a purely collective rotational flow and parameter set 2 which assumes purely radial flow, provided the mean rotational flow energy per nucleon $\langle E_{rot}/A \rangle$ in set 1 and the mean radial flow energy per nucleon $\langle E_r/A \rangle$ in set 2 make equal contributions to the transverse energy; i.e. $2\langle E_r \rangle/3 = \langle E_{rot} \rangle/2$. On the other hand, QMD calculations, both with (dashed lines) and without (crosses) the Pauli potential, and QMD+SMM calculations (dot-dashed lines), for which the collective flow is obtained from the A-body equations of motion, significantly underestimate the transverse energies at

E/A ≥ 55 MeV. The latter tendency is replicated at all other incident energies except E/A=35 MeV where the SMM calculations in Table 1 are consistent with relatively small collective contributions to the transverse energies. Thus the observed fragments manifest a collective transverse expansion that fragments produced by the QMD and QMD+SMM models do not. The origin of this failure is not evident.

The small values of f_E in these SMM model calculations correspond to thermal excitation energies of 5.3-9.0 MeV/nucleon and indicate that the local thermal environment at breakup is much cooler than one would expect if the incident energy were completely thermalized (f_E=1). These excitation energies per nucleon were essentially constrained by the slope parameters τ of the fragment charge distribution. Clearly, neither nature nor the SMM model have any difficulty producing fragmentation events characterized by a slope parameter τ much less than the minimum value τ = 2.3 characteristic of a neutral liquid-gas phase admixture at the critical point. These small slope parameters become even more difficult to accommodate within critical exponent analyses such as those of ref. [3,4,6,7] when one realizes that secondary decay causes the observed charge distributions to be even steeper than those at breakup. The magnitude of this secondary decay correction has been calculated within the SMM approximation, and the calculated charge distributions before secondary decay fitted to obtain the values for τ given by the dotted line in the lower panel of Fig. 2. Clearly, secondary decay makes a significant (close to a factor of 2) correction to the power law parameters for the calculated charge distributions and possibly, to the measured ones as well. Present critical exponent extractions neglect such secondary decay corrections and therefore should be viewed as questionable.

In summary, charge distributions for intermediate mass fragments have been extracted for central ^{84}Kr+^{197}Au collisions at energies ranging from E/A= 35 - 400 MeV. Consistent with recent calculations for finite highly charged systems, the slopes of the fragment charge distributions decrease monotonically with incident energy and at low energies, are characterized by "power laws" with powers much less than those deduced from recent critical exponent extractions. Statistical model calculations indicate moderately low breakup excitation energies, and reveal that post breakup fragment decays alter significantly the observed charge distributions rendering present critical exponent extraction techniques problematic. Dynamical model calculations predict lower fragment multiplicities and transverse energies than are experimentally observed

This work is supported by the National Science Foundation under Grant numbers PHY-90-15255 and PHY-92-14992, and the U.S. Department of Energy under Contract No. DE-FG02-87ER-40316. W.G. Lynch and L.G. Sobotka acknowledge the receipt of U.S. Presidential Young Investigator Awards. J. Pochodzalla acknowledges the financial support of the Deutsche Forschungsgemeinschaft under Contract No. Po 256/2-1.

References:

1. M.E. Fisher, Rep. Prog. Phys. **30** (1967) 615, and refs. therein.
2. K.G. Wilson, Phys. Rev. **B4** (1971) 3174, 3184.
3. X. Campi, Phys. Lett. **B 208** (1988) 351.
4. M.L. Gilkes et al., Phys. Rev. Lett. **73** (1994) 590.
5. D.J. Fields et al., Phys. Lett. **B 187** (1987) 257.
6.. M. Mahi et al., Phys. Rev. Lett. **60** (1988) 1936.
7. T. Li et al., Phys. Rev. Lett. **70** (1993) 1924.
8. J. Pan and S. Das Gupta, Phys. Rev. **C53** (1995) 1319.
9. S. Pratt et al., Phys. Lett. **B 349** (1995) 261.
10. G.J. Kunde et al., to be published.
11. V. Latora et al., Phys. Rev. Lett. **73** (1994) 1765.
12. B. Borderie et al., Phys. Lett. **B 302** (1992) 15.
13. G. Batko and J. Randrup, Nucl. Phys. **A563** (1993) 97.
14. M. D'Agostino et al., Phys. Rev. Lett. **75** (1995) 4373.
15. R.T. de Souza et al., Nucl. Instr. Meth. **A 295** (1990) 109.
16. G.F. Peaslee et al., Phys. Rev. C **49** (1994) R2271.
17. C. Cavata et al., Phys. Rev. C **42** (1990) 1760; Y.D. Kim et al, Phys. Rev. C **45** (1992), 338.
18. G. Peilert et al., Phys. Rev. **C46** (1992) 1457.
19. G. Peilert et al, Phys. Rev. C **39**, 1402 (1989), and refs. therein.
20. P.B. Gossiaux, and J. Aichelin, Rapport Interne SUBATECH - 95 - 04.
21. W.G. Lynch, Nucl. Phys. **A545** (1992) 199c.
22. D.R. Bowman et al., Phys. Rev. C46, (1992) 1834.
23. T.C. Sangster et al, Phys. Rev. **C46** (1992) 1404; J. Konopka, et al., Prog. Part. Nucl. Phys. **30** (1993) 301.
24. A.S. Botvina et al., Nucl. Phys. **A475** (1987) 663; J.P. Bondorf et al., Phys. Rep. **257** (1995) 133.
25. E. Cornell et al., Phys. Rev. Lett. **75** (1995) 1475.
26. M.B. Tsang et al., Phys. Rev. Lett. **57** (1986) 59; A.S. Botvina and D.H.E. Gross, Nucl. Phys. **A475** (1995) 257.

27. S.G. Jeong et al., Phys. Rev. Lett. **72** (1994) 3468; W.C. Hsi et al., Phys. Rev. Lett. **73** (1994) 3367.

28. These collective velocities affect the fragment velocities but not the multiplicities.

29. G.J. Kunde et al., Phys. Rev. Lett. **74** (1995) 38.

Table 1: Parameters of SMM calculations chosen to optimally describe the experimental data.

E_{Beam}/A (MeV)	Set	f_A	f_E	$\langle E_{rot}/A \rangle$ (MeV)	$\langle E_r/A \rangle$ (MeV)
35	1	0.65	0.89	1.2	0.0
35	2	0.65	0.85	0.0	0.9
55	1	0.65	0.76	2.5	0.0
55	2	0.65	0.71	0.0	1.9
70	1	0.60	0.74	4.0	0.0
70	2	0.60	0.67	0.0	3.0
100	1	0.55	0.76	8.0	0.0
100	2	0.55	0.665	0.0	6.0
200	1	0.42	0.585	15.	0.0
200	2	0.42	0.49	0.0	11.
400	1	0.32	0.44	25.	0.0
400	2	0.32	0.36	0.0	19.

Figure Captions:

Fig. 1. Probabilities of emitting fragments of charge Z per collision (solid points) and power law fits for central $^{84}Kr+^{197}Au$ collisions as functions of the incident energy per nucleon.

Fig. 2. Experimental and theoretical fragment multiplicities (upper panel) and power law parameters τ ($Y \propto Z^{-\tau}$; lower panel) for central $^{84}Kr+^{197}Au$ collisions as functions of the incident energy per nucleon. The various symbols are explained in the text and in the internal figure caption.(Theoretical uncertainties in τ or $<N_{IMF}>$ are typically ± 0.2.)

Fig. 3. Experimental and theoretical fragment transverse momenta for central $^{84}Kr+^{197}Au$ collisions as functions of the incident energy per nucleon. The various symbols are explained in the text and the internal figure caption. Uncertainties in the calculated values of $<E_t>$, shown in the case of the SMM model, are essentially the same for other models.

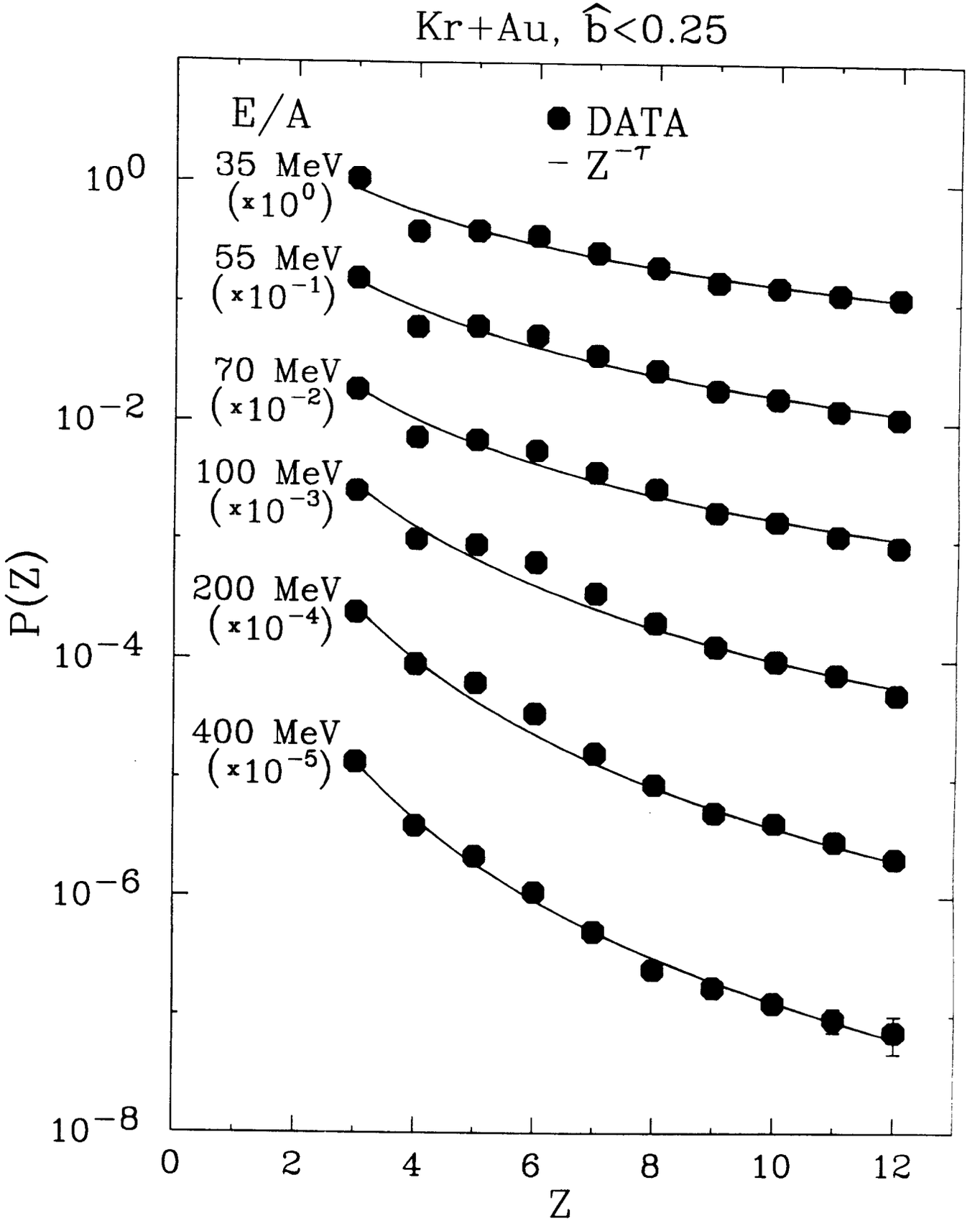
Kr+Au, $\hat{b}$<0.25
E/A
DATA
$- Z^{-\tau}$
35 MeV
(×10^0)
55 MeV
(×10^-1)
70 MeV
(×10^-2)
100 MeV
(×10^-3)
200 MeV
(×10^-4)
400 MeV
(×10^-5)
P(Z)
10^0
10^-2
10^-4
10^-6
10^-8
0
2
4
6
8
10
12
Z

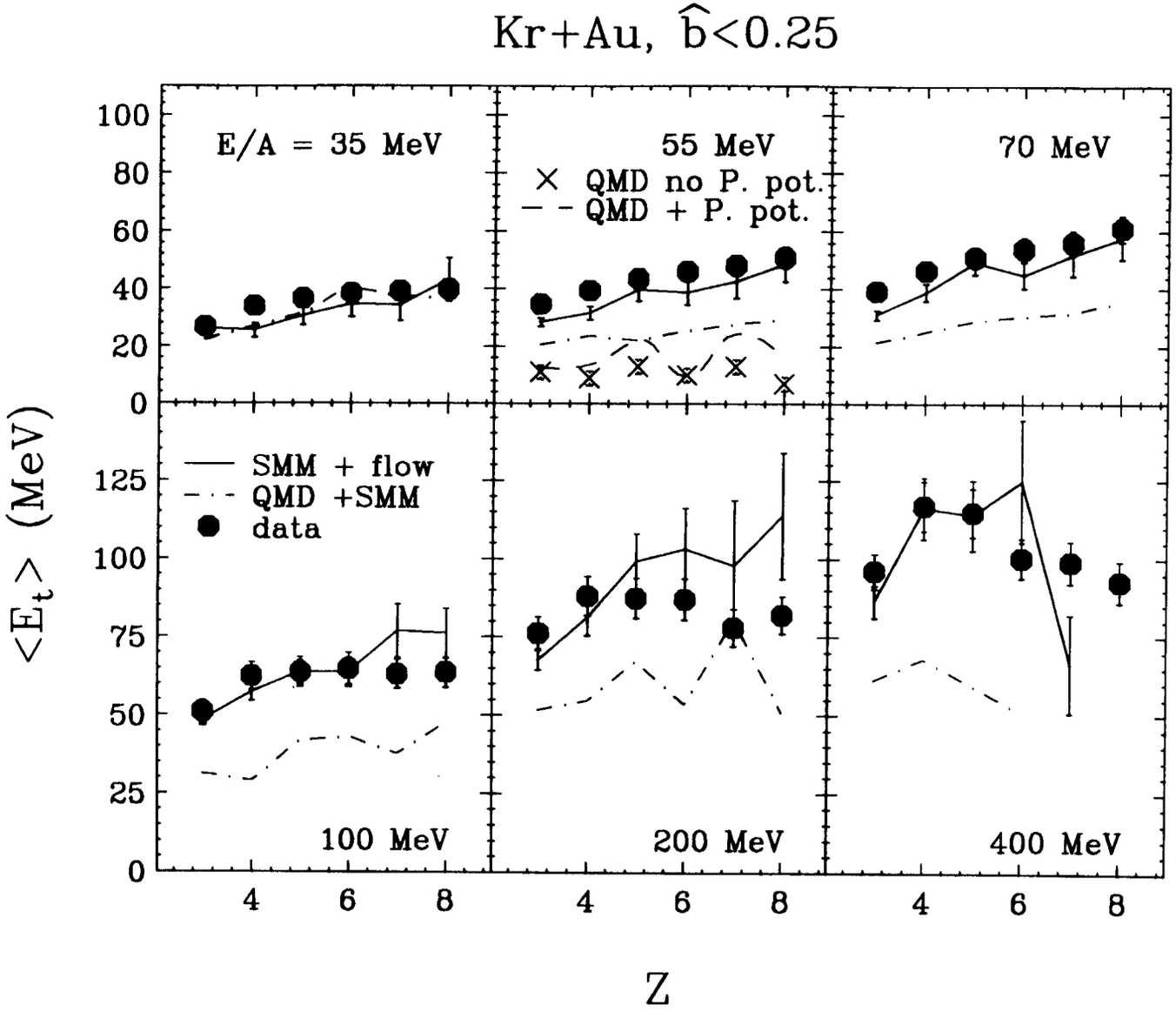
Kr+Au, $\hat{b}$<0.25
E/A = 35 MeV
55 MeV
70 MeV
× QMD no P. pot.
– – QMD + P. pot.
SMM + flow
QMD +SMM
data
100 MeV
200 MeV
400 MeV
<E_t> (MeV)
Z

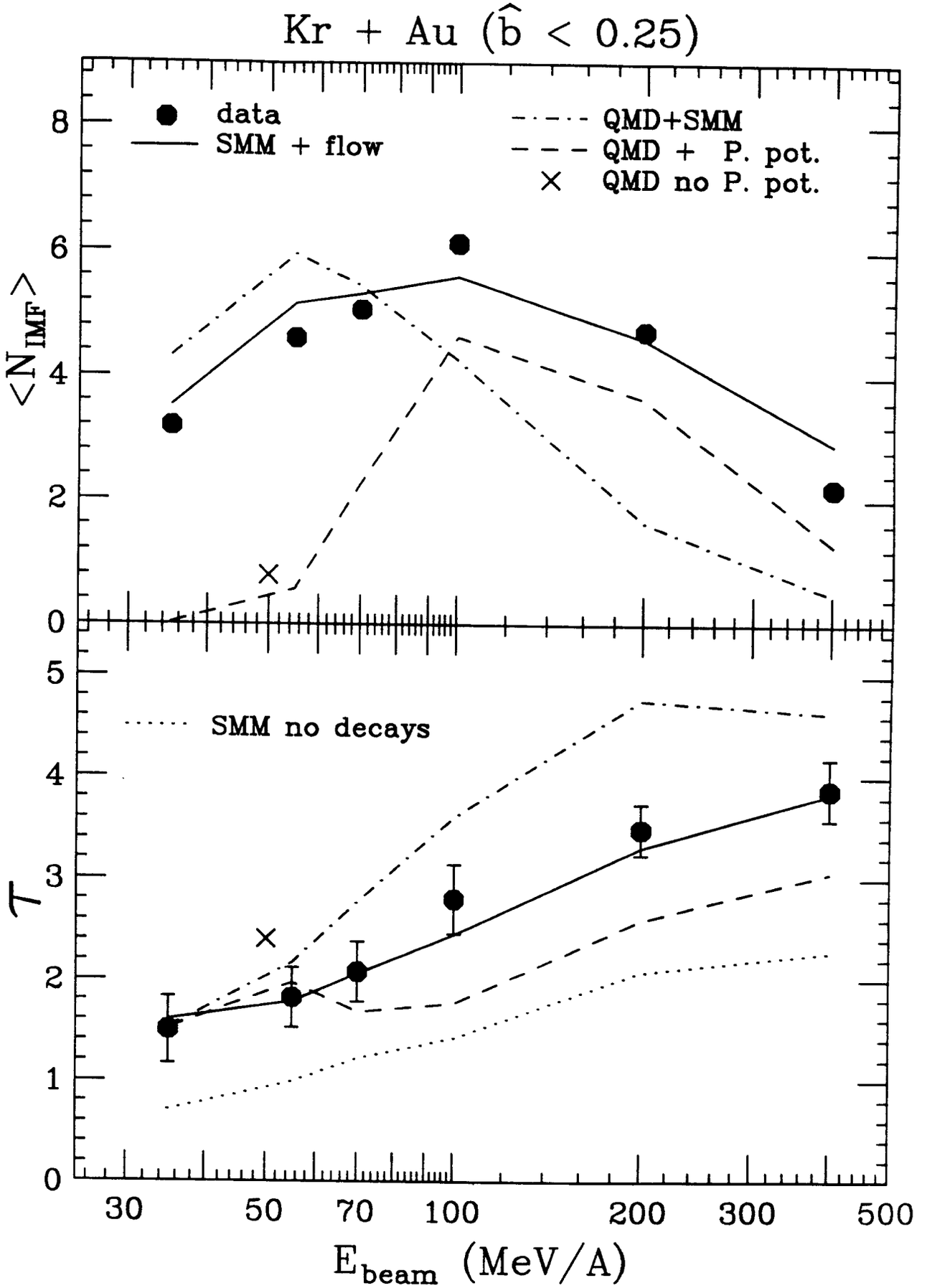
Kr + Au ($\hat{b}$ < 0.25)
data
SMM + flow
QMD+SMM
QMD + P. pot.
QMD no P. pot.
$\langle N_{IMF} \rangle$
SMM no decays
τ
E_{beam} (MeV/A)

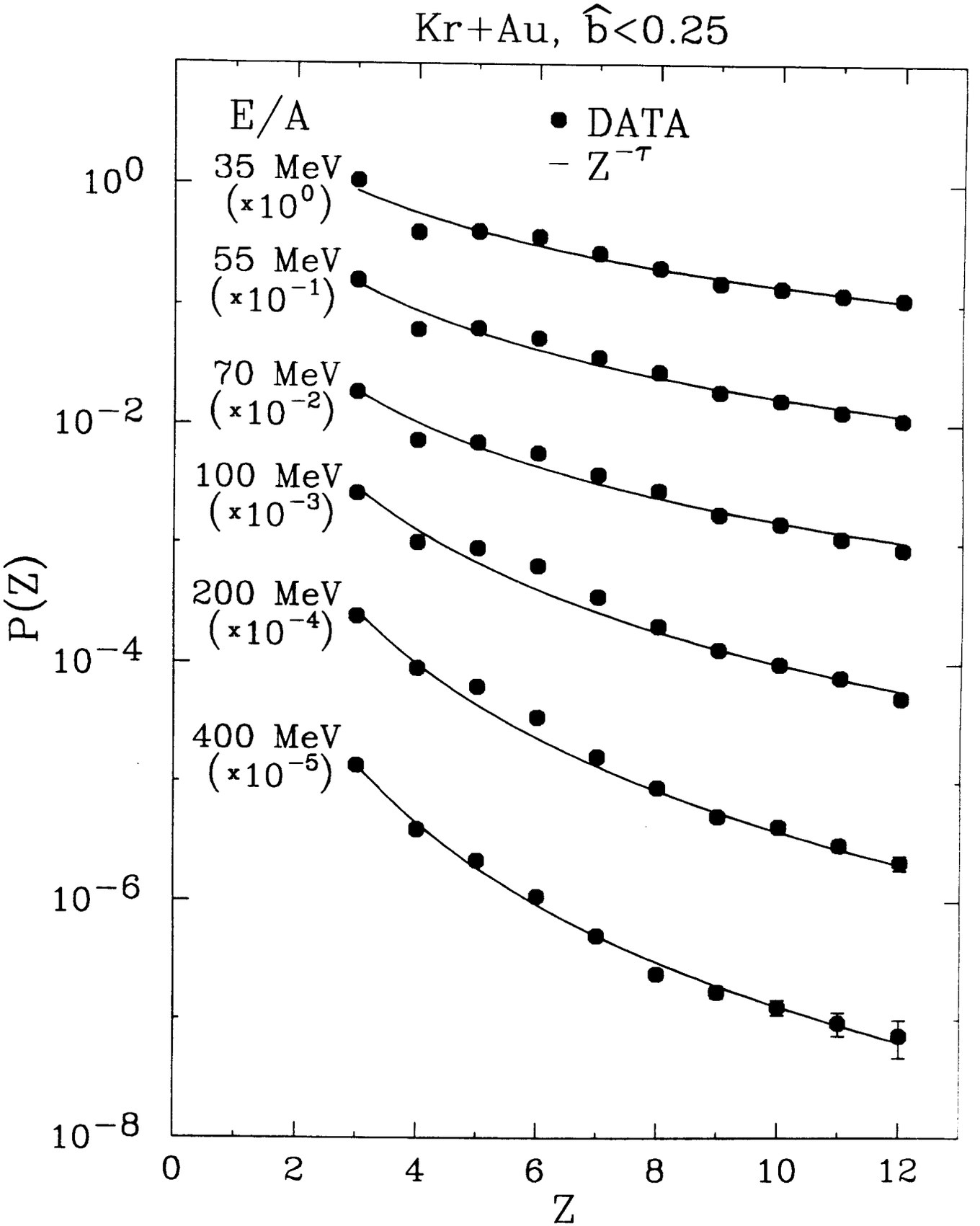
Kr+Au, $\hat{b}$<0.25
E/A
DATA
$-Z^{-\tau}$
35 MeV
(×10^0)
55 MeV
(×10^-1)
70 MeV
(×10^-2)
100 MeV
(×10^-3)
200 MeV
(×10^-4)
400 MeV
(×10^-5)
P(Z)
10^0
10^-2
10^-4
10^-6
10^-8
0
2
4
6
8
10
12
Z